



Quantum model of microcavity intersubband electroluminescent devices

Simone de Liberato, Cristiano Ciuti

► To cite this version:

Simone de Liberato, Cristiano Ciuti. Quantum model of microcavity intersubband electroluminescent devices. *Physical Review B: Condensed Matter and Materials Physics* (1998-2015), 2008, 77, pp.155321. hal-00189235v2

HAL Id: hal-00189235

<https://hal.science/hal-00189235v2>

Submitted on 28 Apr 2008

HAL is a multi-disciplinary open access archive for the deposit and dissemination of scientific research documents, whether they are published or not. The documents may come from teaching and research institutions in France or abroad, or from public or private research centers.

L'archive ouverte pluridisciplinaire **HAL**, est destinée au dépôt et à la diffusion de documents scientifiques de niveau recherche, publiés ou non, émanant des établissements d'enseignement et de recherche français ou étrangers, des laboratoires publics ou privés.

Quantum model of microcavity intersubband electroluminescent devices

Simone De Liberato^{1,2} and Cristiano Ciuti^{1*}

¹*Laboratoire Matériaux et Phénomènes Quantiques,
Université Paris Diderot-Paris 7 and CNRS, UMR 7162,
Bâtiment Condorcet, 75205 Paris Cedex 13, France and*

²*Laboratoire Pierre Aigrain, École Normale Supérieure, 24 rue Lhomond, 75005 Paris, France*

We present a quantum theoretical analysis of the electroluminescence from an intersubband transition of a quantum well structure embedded in a planar microcavity. By using a cluster factorization method, we have derived a closed set of dynamical equations for the quantum well carrier and cavity photon occupation numbers, the correlation between the cavity field and the intersubband polarization, as well as polarization-polarization contributions. In order to model the electrical excitation, we have considered electron population tunneling from an injector and into an extractor contact. The tunneling rates have been obtained by considering the bare electronic states in the quantum well and the limit of validity of this approximation (broad-band injection) are discussed in detail. We apply the present quantum model to provide a comprehensive description of the electronic transport and optical properties of an intersubband microcavity light emitting diode, accounting for non-radiative carrier relaxation and Pauli blocking. We study the enhancement of the electroluminescence quantum efficiency passing from the weak to the strong polariton coupling regime and compare it with the free-space case.

In the last two decades, the fundamental research on the physics of intersubband transitions in semiconductor quantum wells has enjoyed a considerable success and also led to novel applications in quantum optoelectronics[1]. Recently, reflectivity experiments [2, 3, 4] have demonstrated that by embedding a doped quantum well structure in a planar microcavity, it is possible to achieve the strong coupling regime between an intersubband transition and a cavity photon mode, provided that a dense enough two-dimensional electron gas populates the fundamental quantum well subband. The interaction between a bright intersubband excitation and a cavity photon is quantified by the so-called vacuum Rabi frequency. The strong coupling regime occurs when the vacuum Rabi frequency exceeds the electronic and photonic losses. In such a regime, the normal modes of the system are cavity polaritons, half-photon half-intersubband excitations. In this kind of system, it is even possible to reach an unconventional ultra-strong coupling regime, i.e. a vacuum Rabi frequency comparable to the intersubband transition frequency[5, 6, 7].

The interplay between judiciously quantum engineered intersubband transitions and vertical electron transport is the essence of the so-called quantum cascade electroluminescent devices and lasers, which are unipolar optoelectronic sources emitting in the mid and far infrared portion of the electromagnetic spectrum [8, 9, 10]. A new kind of microcavity-embedded quantum cascade devices in the strong coupling regime was proposed in Ref. 11. The first experimental demonstrations of a microcavity quantum cascade photovoltaic detector[12] and of an electroluminescent device in the strong coupling regime have been recently reported[13].

This promising research topic is in its very infancy and many interesting theoretical questions need to be addressed. In Ref. 6, intersubband polariton electroluminescence has been analytically treated within a simplified Hamiltonian model based on the following assumptions: (i) only the bright intersubband excitations have been taken into account, while dark excitations have been neglected; (ii) only the low excitation regime has been considered, in which the bright intersubband excitations have been approximated as bosons; (iii) the electronic coupling to the intersubband polarization field has been modeled through a phenomenological reservoir of bosonic excitations. In this work, we will attempt to treat the same problem starting directly from the fermionic Hamiltonian for the quantum well carriers. This approach can give us useful insight to understand the physics obtained by relaxing the assumptions used in Ref. 6 and to grasp which intrinsic factors ultimately determine the quantum efficiency of these strong coupling emitters. On one hand, the large values of the vacuum Rabi frequency could induce a very fast and efficient emission of photons. On the other hand, the large density of dark intersubband excitations created by the injection current and the Pauli blocking in the densely populated fundamental subband could suppress such enhancement.

We would like to point out that from a theoretical point of view, a description of the considered system in terms of the fermionic carrier operators makes the system Hilbert space much larger than within a bosonic model. In this paper, we have followed an approach based on a truncation of the infinite hierarchy of dynamical equations for the operator expectation values, allowing us to describe many relevant aspects of the intersubband microcavity electroluminescence. However, some of the non-perturbative features obtained analytically within a bosonic model[6] can not be accounted for within the present treatment. Different fermionic approaches based

*Electronic address: cristiano.ciuti@univ-paris-diderot.fr

on exact diagonalization methods [14] are eventually necessary for further refinements.

In this paper, we present a quantum model of the spontaneous photon emission from an electrically-excited intersubband transition of a quantum well structure embedded in a planar microcavity mode. Here, we will consider the case of an incoherent electron transport, where the quantum well electron populations in the two subbands have a tunneling coupling to an electronic injector and to an extractor. The tunneling rates have been obtained by considering the bare electron states inside the quantum well. The domain of validity of this approximation will be discussed in detail. The present theoretical model is applied to describe the incoherent electron transport and electroluminescence of an intersubband microcavity light emitting diode in the strong coupling regime. The paper is structured as follows. In Sec. I, we describe the system and introduce the second quantization Hamiltonian describing electrons in the two conduction subbands and photons in the fundamental microcavity mode. In Sec. II, we present a closed set of dynamical equations for the one-time expectation values of operator products, describing photon and carrier populations as well as intersubband polarization-polarization and polarization-field correlations. These equations have been obtained through a cluster expansion, whose de-

tails are reported in Appendix A. In Sec. III, we discuss the steady-state regime obtained under constant electrical excitation. The corresponding set of algebraic equations for the steady-state expectation values are reported in Appendix B. In Sec. IV, the electroluminescence spectra are analytically calculated as a function of the populations and the appearance of intersubband cavity polaritonic resonances in the emission spectra is shown. Numerical applications of the theory are presented in Sec. V, using a specific configuration for the injection and extraction electronic reservoirs. The results predict the current-voltage characteristics, emission spectra and quantum efficiency using different (controllable) parameters for the considered microcavity system. The results are critically discussed with respect to the approximations of the model. Finally, conclusions and future perspectives are drawn in Sec. VI.

I. DESCRIPTION OF THE SYSTEM AND QUANTUM HAMILTONIAN

The system under study is described by the following second quantization Hamiltonian

$$H = \sum_{\mathbf{k},\sigma} \hbar\omega_1(\mathbf{k})c_{1,\sigma,\mathbf{k}}^\dagger c_{1,\sigma,\mathbf{k}} + \sum_{\mathbf{k},\sigma} \hbar\omega_2(\mathbf{k})c_{2,\sigma,\mathbf{k}}^\dagger c_{2,\sigma,\mathbf{k}} + \sum_{\mathbf{k}} \hbar\omega_c(\mathbf{k})a_{\mathbf{k}}^\dagger a_{\mathbf{k}} + \sum_{\mathbf{k},\mathbf{q},\sigma} \hbar\chi(\mathbf{q})a_{\mathbf{q}}c_{1,\sigma,\mathbf{k}}c_{2,\sigma,\mathbf{k}+\mathbf{q}}^\dagger + \sum_{\mathbf{k},\mathbf{q},\sigma} \hbar\chi^*(\mathbf{q})a_{\mathbf{q}}^\dagger c_{2,\sigma,\mathbf{k}+\mathbf{q}}c_{1,\sigma,\mathbf{k}}^\dagger + H_{other}. \quad (1)$$

The energy dispersions of the two quantum well conduction subbands are $\hbar\omega_1(\mathbf{k}) = \frac{\hbar^2 k^2}{2m^*}$ and $\hbar\omega_2(\mathbf{k}) = E_{12} + \frac{\hbar^2 k^2}{2m^*}$, being \mathbf{k} the electron in-plane wavevector and m^* the effective mass (non-parabolicity is here neglected). The corresponding electron creation fermionic operators are $c_{1,\sigma,\mathbf{k}}^\dagger$ and $c_{2,\sigma,\mathbf{k}}^\dagger$, where σ is the electron spin. $\omega_c(\mathbf{q}) = \frac{c}{\sqrt{\epsilon_r}}\sqrt{q_z^2 + q^2}$ is the bare frequency dispersion of a cavity photonic branch as a function of the in-plane wavevector \mathbf{q} , where c is the light speed, ϵ_r is the cavity spacer dielectric constant and q_z is the quantized photon wavevector along the normal direction. $a_{\mathbf{q}}^\dagger$ is the corresponding photon creation operator, obeying bosonic commutation rules. Due to the well-known polarization selection rules of intersubband transitions, we omit the photon polarization, which is assumed to be Transverse Magnetic (TM). For simplicity, we consider only a photonic branch, which is quasi-resonant with the intersubband transition, while other cavity photon modes are supposed to be off-resonance and can be therefore neglected in first approximation. The interaction between

the cavity photon field and the two electronic subbands is quantified by the coupling constant

$$\chi(\mathbf{q}) = \sqrt{\frac{\omega_{12}^2 d_{12}^2}{\hbar\epsilon_0\epsilon_r L_{cav} S \omega_c(\mathbf{q})} \frac{q^2}{(\pi/L_{cav})^2 + q^2}}, \quad (2)$$

where d_{12} is the intersubband transition dipole along the quantum well growth direction, $\omega_{12} = E_{12}/\hbar$ is the frequency of the intersubband transition, ϵ_0 the vacuum permittivity, L_{cav} is the effective cavity length and S is the sample area. For simplicity, we have considered a $\lambda/2$ -cavity, with $q_z = \pi/L_{cav}$ being the quantized vector along the growth direction. The geometrical factor $\frac{q^2}{(\pi/L_{cav})^2 + q^2}$ originates from the TM-polarization nature of the transition. Moreover, in Eq. (2) we have assumed that the active quantum well is located at the antinode of the cavity mode field, providing maximum coupling. Note that here we have neglected the anti-resonant terms of the light-matter interaction and therefore we can describe the strong coupling regime for the electrically excited system, but not the ultrastrong coupling limit, as

instead done in Refs. 5, 6, 7. The Hamiltonian term H_{other} is meant to include all the other interactions: (i) electron-phonon interaction; (ii) electron-electron interaction; (iii) electron tunneling coupling to the injection and extraction reservoir; (iv) coupling between the cavity photon field and the extracavity field.

II. CLOSED SET OF DYNAMICAL EQUATIONS FOR THE ONE-TIME EXPECTATION VALUES

It is known that due to the cubic light-matter coupling term in the Hamiltonian (the product of two fermion operators and one boson operator) it is not possible to write down an exact closed set of equations for the evolution of operators, being the Heisenberg equation of motion for each product of N operators coupled at least with one product of $N + 1$ operators. In other words, the equations of motion of the different observables of the system form an infinite hierarchy. One approximation method that has been used in order to solve this kind of systems is the so-called cluster expansion scheme[15, 16, 17]. It is based on a systematic development of expectation values of operator products in terms of correlation functions.

In order to obtain a consistent truncation scheme, a pair of fermionic operators has to be considered of the same order as a single bosonic operator. In this work, we have truncated the hierarchy at the level of the product of two excitation operators (i.e., the product of four fermion operators). The details of the factorization are in Appendix A. The expectation values entering the present cluster factorization are the electronic and photonic populations, the correlation between the cavity photon field and the intersubband polarization, as well as polarization-polarization correlations. The electron occupation numbers in the two quantum well conduction subbands are $n_{1,\mathbf{k}} = \langle c_{1,\sigma,\mathbf{k}}^\dagger c_{1,\sigma,\mathbf{k}} \rangle$ and $n_{2,\mathbf{k}} = \langle c_{2,\sigma,\mathbf{k}}^\dagger c_{2,\sigma,\mathbf{k}} \rangle$. Note that, since in the absence of a magnetic field all quantities are spin-independent, we omit the spin-index in the notation of the averaged quantities. The cavity photon number is $n_{a,\mathbf{q}} = \langle a_{\mathbf{q}}^\dagger a_{\mathbf{q}} \rangle$. The correlation between the cavity photon field and the intersubband electronic polarization is represented by the quantity

$$Y(\mathbf{q}, \mathbf{k}) = \langle a_{\mathbf{q}}^\dagger c_{1,\sigma,\mathbf{k}}^\dagger c_{2,\sigma,\mathbf{k}+\mathbf{q}} \rangle. \quad (3)$$

Finally, the polarization-polarization correlation function is given by

$$X(\mathbf{q} + \mathbf{k}', \mathbf{k}', \mathbf{k}) = \sum_{\sigma} \langle c_{2,\sigma,\mathbf{q}+\mathbf{k}'}^\dagger c_{1,\sigma,\mathbf{k}'}^\dagger c_{1,\sigma',\mathbf{k}}^\dagger c_{2,\sigma',\mathbf{k}+\mathbf{q}} \rangle. \quad (4)$$

Note that in the spontaneous photon emission regime, $Y(\mathbf{q}, \mathbf{k})$ can not be factorized: in fact, spontaneous emis-

sion is incoherent and $\langle a_{\mathbf{q}} \rangle = 0$, $\langle c_{1,\sigma,\mathbf{k}}^\dagger c_{2,\sigma,\mathbf{k}+\mathbf{q}} \rangle = 0$, meaning that the cavity field and the intersubband polarization have no definite phase. Loss of coherence due to dephasing processes and photonic losses is phenomenologically quantified by the damping rate Γ_Y . Unlike $Y(\mathbf{q}, \mathbf{k})$, $X(\mathbf{k}' + \mathbf{q}, \mathbf{k}', \mathbf{k})$ can be factorized in products of non-zero lower-order expectation values of operators. In fact, we have $X(\mathbf{k}' + \mathbf{q}, \mathbf{k}', \mathbf{k}) = 2n_{2,\mathbf{k}+\mathbf{q}}(1 - n_{1,\mathbf{k}})\delta_{\mathbf{k},\mathbf{k}'} + \delta X(\mathbf{k}' + \mathbf{q}, \mathbf{k}', \mathbf{k})$. The first contribution is an uncorrelated plasma term, while $\delta X(\mathbf{k}' + \mathbf{q}, \mathbf{k}', \mathbf{k})$ describes the higher-order correlation, which can be destroyed by dephasing processes quantified by the damping rate Γ_X .

The terms in H_{other} , namely the phonon scattering, electron-electron interaction, the coupling to the contact reservoirs and the coupling to the external electromagnetic field will be treated in an effective way. The carrier non-radiative relaxation (due to phonon-electron and electron-electron scattering) is modeled in terms of a simple phenomenological relaxation time $\tau_{\mathbf{k}}$. Note that the role of Coulomb electron-electron interaction on intersubband transitions has been studied, e.g., in Ref. 19. In the case of subbands with parallel parabolic dispersion (e.g., same effective mass), Coulomb interaction produces a moderate renormalization of the intersubband transition frequency ω_{12} and of its oscillator strength, which will not be accounted explicitly in the present work.

Let $n_{1,\mathbf{k}}^0$ and $n_{2,\mathbf{k}}^0$ be the self-consistent local equilibrium occupation numbers. They are given by Fermi-Dirac distributions:

$$\begin{aligned} n_{1,\mathbf{k}}^0 &= \frac{1}{e^{\beta(\hbar\omega_1(\mathbf{k}) - \epsilon_F)} + 1}, \\ n_{2,\mathbf{k}}^0 &= \frac{1}{e^{\beta(\hbar\omega_2(\mathbf{k}) - \epsilon_F)} + 1}, \end{aligned} \quad (5)$$

where $\beta = 1/(KT)$ is the Boltzmann thermal factor, and ϵ_F is the quantum well self-consistent Fermi level, such that:

$$\sum_{\mathbf{k}} n_{1,\mathbf{k}} + n_{2,\mathbf{k}} = \frac{Sm^*}{2\pi\hbar^2} \int_0^\infty d\epsilon \frac{1}{e^{\beta(\epsilon - \epsilon_F)} + 1} + \frac{1}{e^{\beta(\epsilon + E_{12} - \epsilon_F)} + 1}. \quad (6)$$

The two subbands are coupled to two electronic reservoirs, named respectively left and right contacts. We will call $\Gamma_{p,j,\mathbf{k}}^{in}$ the electronic tunneling rate into the \mathbf{k} -mode of the subband $j = 1, 2$ from the reservoir $p = \text{left, right}$. Analogously $\Gamma_{p,j,\mathbf{k}}^{out}$ is defined as the electronic tunneling rate from the \mathbf{k} -mode of the subband j into the reservoir p . The total in-tunneling and out-tunneling rates are $\Gamma_{j,\mathbf{k}}^{in} = \Gamma_{\text{left},j,\mathbf{k}}^{in} + \Gamma_{\text{right},j,\mathbf{k}}^{in}$ and $\Gamma_{j,\mathbf{k}}^{out} = \Gamma_{\text{left},j,\mathbf{k}}^{out} + \Gamma_{\text{right},j,\mathbf{k}}^{out}$.

The resulting closed system of equations for the one-time expectation values reads:

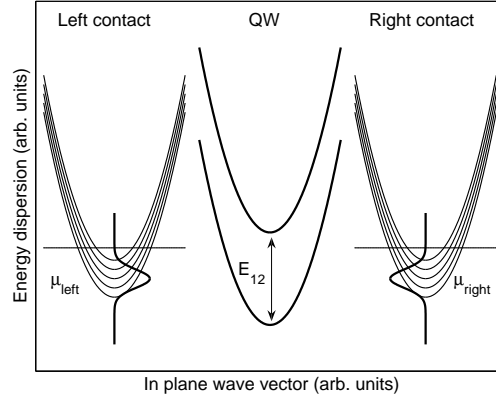


FIG. 1: Sketch of the energy dispersion of the two quantum well subbands and of the minibands in the left and right contacts in the zero-bias case. Here the system is in thermal equilibrium and the Fermi level in the quantum well is the same as in the two contacts. The doping level in the contacts determines the equilibrium density in the quantum well. The subband and minibands have an energy dispersion versus the in-plane wavevector, which is a conserved quantity in the planar structure. This electronic structure is embedded in a planar microcavity, with a cavity photon mode quasi-resonant to the intersubband transition.

$$\begin{aligned}
\frac{d}{dt}n_{a,\mathbf{q}} &= -2\gamma n_{a,\mathbf{q}} + 2i \sum_{\mathbf{k}} \chi^*(\mathbf{q})Y(\mathbf{q},\mathbf{k}) + c.c. \\
\frac{d}{dt}n_{1,\mathbf{k}} &= -\frac{n_{1,\mathbf{k}} - n_{1,\mathbf{k}}^0}{\tau_{\mathbf{k}}} - \Gamma_{1,\mathbf{k}}^{out}n_{1,\mathbf{k}} + \Gamma_{1,\mathbf{k}}^{in}(1 - n_{1,\mathbf{k}}) + i \sum_{\mathbf{q}} \chi^*(\mathbf{q})Y(\mathbf{q},\mathbf{k}) + c.c. \\
\frac{d}{dt}n_{2,\mathbf{k}} &= -\frac{n_{2,\mathbf{k}} - n_{2,\mathbf{k}}^0}{\tau_{\mathbf{k}}} - \Gamma_{2,\mathbf{k}}^{out}n_{2,\mathbf{k}} + \Gamma_{2,\mathbf{k}}^{in}(1 - n_{2,\mathbf{k}}) - i \sum_{\mathbf{q}} \chi^*(\mathbf{q})Y(\mathbf{q},\mathbf{k} - \mathbf{q}) + c.c. \\
\frac{d}{dt}Y(\mathbf{q},\mathbf{k}) &= i(\omega_c(\mathbf{q}) + \omega_1(\mathbf{k}) - \omega_2(\mathbf{k} + \mathbf{q}) + i\Gamma_Y(\mathbf{q},\mathbf{k}))Y(\mathbf{q},\mathbf{k}) \\
&\quad - i \sum_{\mathbf{q}'} \chi(\mathbf{q})X(\mathbf{q} + \mathbf{q}',\mathbf{q}',\mathbf{k}) + i\chi(\mathbf{q})n_{a,\mathbf{q}}(n_{1,\mathbf{k}} - n_{2,\mathbf{k}+\mathbf{q}}) \\
\frac{d}{dt}X(\mathbf{k}' + \mathbf{q},\mathbf{k}',\mathbf{k}) &= i(-\omega_1(\mathbf{k}') + \omega_2(\mathbf{k}' + \mathbf{q}) + \omega_1(\mathbf{k}) - \omega_2(\mathbf{k} + \mathbf{q}))X(\mathbf{k}' + \mathbf{q},\mathbf{k}',\mathbf{k}) \\
&\quad - \Gamma_X(\mathbf{k}' + \mathbf{q},\mathbf{k}',\mathbf{k})(X(\mathbf{k}' + \mathbf{q},\mathbf{k}',\mathbf{k}) - 2n_{2,\mathbf{k}+\mathbf{q}}(1 - n_{1,\mathbf{k}})\delta_{\mathbf{k},\mathbf{k}'}) \\
&\quad + i \sum_{\mathbf{q}'} \chi(\mathbf{q}') (Y^*(\mathbf{q}',\mathbf{k})\delta_{\mathbf{k}',\mathbf{k}}n_{2,\mathbf{k}+\mathbf{q}} + Y^*(\mathbf{q}',\mathbf{q} + \mathbf{k} - \mathbf{q}')\delta_{\mathbf{k}',\mathbf{k}}(1 - n_{1,\mathbf{k}})) \\
&\quad + 2i\chi(\mathbf{q})Y^*(\mathbf{q},\mathbf{k}') (n_{1,\mathbf{k}} - n_{2,\mathbf{k}+\mathbf{q}}) - 2i\chi^*(\mathbf{q})Y(\mathbf{q},\mathbf{k})(n_{1,\mathbf{k}'} - n_{2,\mathbf{k}'+\mathbf{q}}).
\end{aligned} \tag{7}$$

A. Injection and extraction tunneling rates

The wave-vector dependent injection and extraction rates in Eq. (7) can be in principle of different origin. Here we give the formal expression for elastic tunneling processes conserving the in-plane momentum. Additional processes (such as assisted tunneling) can be ac-

counted for by adding their contribution to the expressions for $\Gamma_{j,\mathbf{k}}^{in}$ and $\Gamma_{j,\mathbf{k}}^{out}$ to be inserted in Eq. (7).

As electronic contact reservoirs, we will consider semiconductor doped superlattices, as it is generally the case in unipolar quantum cascade devices.

The chemical potential in each contact is labeled μ_p with $p = \text{left, right}$. In each reservoir, we will consider miniband states with energy $E_{p,\mathbf{k},k_z}^{res}$. In the elastic tun-

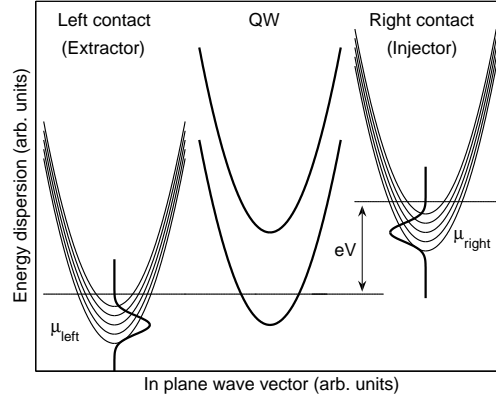


FIG. 2: Same as in Fig. 1, but with an applied voltage bias. Here, the left contact acts as an electronic extractor, while the right one is the injector. In the quantum well, non-equilibrium steady-state populations can be established in the two subbands.

neling process, electron energy and in-plane momentum are conserved. The tunneling rate from the contact reservoir into the j -th subband is

$$\Gamma_{p,j,\mathbf{k}}^{in} = \frac{2\pi}{\hbar} \sum_{k_z} \frac{|V_{p,j,\mathbf{k},k_z}|^2 \delta(E_{p,\mathbf{k},k_z}^{res} - \hbar\omega_j(\mathbf{k}))}{1 + e^{\beta(E_{p,\mathbf{k},k_z}^{res} - \mu_p)}}, \quad (8)$$

where V_{p,j,\mathbf{k},k_z} is the tunneling matrix element and k_z is in general an index over the electronic states of the miniband with in-plane wave vector \mathbf{k} . It can be interpreted as the axial electronic wave vector in the case the two leads are just bulk contacts. $1/(1 + e^{\beta(E_{p,\mathbf{k},k_z}^{res} - \mu_p)})$ is the Fermi-Dirac occupation number of the electron states in the contact. Analogously the tunneling rate from the j -th subband of the quantum well into the reservoir p reads

$$\Gamma_{p,j,\mathbf{k}}^{out} = \frac{2\pi}{\hbar} \sum_{k_z} \frac{|V_{p,j,\mathbf{k},k_z}|^2 \delta(E_{p,\mathbf{k},k_z}^{res} - \hbar\omega_j(\mathbf{k}))}{1 + e^{-\beta(E_{p,\mathbf{k},k_z}^{res} - \mu_p)}}, \quad (9)$$

where $1/(1 + e^{-\beta(E_{p,\mathbf{k},k_z}^{res} - \mu_p)}) = 1 - 1/(1 + e^{\beta(E_{p,\mathbf{k},k_z}^{res} - \mu_p)})$ is the hole occupation number in the contact. The value of $\Gamma_{p,j,\mathbf{k}}^{in,out}$ can be quantum engineered, depending on the specific structure. In particular, by changing the thickness of the potential barriers, it is possible to tailor considerably the tunneling matrix element. It is straightforward to see that a simple relationship occurs between $\Gamma_{p,j,\mathbf{k}}^{in}$ and $\Gamma_{p,j,\mathbf{k}}^{out}$, namely

$$\frac{\Gamma_{p,j,\mathbf{k}}^{in}}{\Gamma_{p,j,\mathbf{k}}^{out}} = e^{\beta(\mu_p - \hbar\omega_j(\mathbf{k}))}. \quad (10)$$

Note that here we have assumed that the bare energy dispersion of the electrons in the two subbands is unaffected. This is valid in the weak light-matter coupling regime or when the injector miniband energy width is

broad enough. For large values of the vacuum Rabi frequency, the spectral function of the electrons in the second subband is non-trivially modified as well as the tunneling process using a narrow-band injector. This will be proved and discussed in detail in a forthcoming paper[14].

III. STEADY-STATE REGIME AND OBSERVABLE QUANTITIES

In this work, we will focus on the steady-state solutions for the quantities $n_{a,\mathbf{q}}$, $n_{1,\mathbf{k}}$, $n_{2,\mathbf{k}}$, $Y(\mathbf{q},\mathbf{k})$ and $X(\mathbf{q} + \mathbf{q}', \mathbf{q}', \mathbf{k})$. Hence, we can set the time derivatives equal to zero, transforming the differential system (7) into an algebraic one. In the steady-state regime, the electronic current (number of electrons per unit time) through the structure is given by the expression:

$$\begin{aligned} I &= \sum_{\mathbf{k}} \Gamma_{1,\mathbf{k}}^{out} n_{1,\mathbf{k}} - \Gamma_{1,\mathbf{k}}^{in} (1 - n_{1,\mathbf{k}}) \\ &= \sum_{\mathbf{k}} \Gamma_{2,\mathbf{k}}^{in} (1 - n_{2,\mathbf{k}}) - \Gamma_{2,\mathbf{k}}^{out} n_{2,\mathbf{k}}. \end{aligned} \quad (11)$$

The total rate of photons emitted out of the microcavity reads

$$P = 2\gamma \sum_{\mathbf{q}} n_{a,\mathbf{q}}, \quad (12)$$

where $1/(2\gamma)$ is the escape time of a photon out of the microcavity. The *quantum efficiency* η is defined as the ratio between the photonic current out of the cavity and electronic current, i.e., $\eta = \frac{P}{I}$.

IV. EMISSION SPECTRA

In the steady-state regime, the momentum-dependent spontaneous photon emission spectra are given by the

expression:

$$\mathcal{L}_{\mathbf{q}}(\omega) \propto \int_0^\infty dt \Re \langle a_{\mathbf{q}}^\dagger(0) a_{\mathbf{q}}(t) \rangle e^{(i\omega - 0^+)t}. \quad (13)$$

In order to determine $\langle a_{\mathbf{q}}^\dagger(0) a_{\mathbf{q}}(t) \rangle$, we need to solve the following Heisenberg equations of motion

$$\frac{d}{dt} \langle a_{\mathbf{q}}^\dagger(0) a_{\mathbf{q}} \rangle = -i\omega_c(\mathbf{q}) \langle a_{\mathbf{q}}^\dagger(0) a_{\mathbf{q}} \rangle + i\chi^*(\mathbf{q}) \sum_{\mathbf{k}, \sigma} \langle a_{\mathbf{q}}^\dagger(0) c_{1,\sigma,\mathbf{k}}^\dagger c_{2,\sigma,\mathbf{k}+\mathbf{q}} \rangle \quad (14)$$

$$\begin{aligned} \frac{d}{dt} \langle a_{\mathbf{q}}^\dagger(0) c_{1,\sigma,\mathbf{k}}^\dagger c_{2,\sigma,\mathbf{k}+\mathbf{q}} \rangle &= -i\omega_{12} \langle a_{\mathbf{q}}^\dagger(0) c_{1,\sigma,\mathbf{k}}^\dagger c_{2,\sigma,\mathbf{k}+\mathbf{q}} \rangle \\ &\quad - i \sum_{\mathbf{q}'} \chi(\mathbf{q}') \langle a_{\mathbf{q}}^\dagger(0) a_{\mathbf{q}'} c_{2,\sigma,\mathbf{k}+\mathbf{q}'}^\dagger c_{2,\sigma,\mathbf{k}+\mathbf{q}} \rangle + i \sum_{\mathbf{q}'} \chi(\mathbf{q}') \langle a_{\mathbf{q}}^\dagger(0) a_{\mathbf{q}'} c_{1,\sigma,\mathbf{k}}^\dagger c_{1,\sigma,\mathbf{k}+\mathbf{q}-\mathbf{q}'} \rangle. \end{aligned}$$

Note that here we have omitted the coupling of the electronic injector and extractor reservoirs to the quantity $\langle a_{\mathbf{q}}^\dagger(0) c_{1,\sigma,\mathbf{k}}^\dagger c_{2,\sigma,\mathbf{k}+\mathbf{q}} \rangle$. This coupling would involve correlations between the quantum well electronic field and the contact electronic fields. Since in this paper we are dealing with incoherent electron transport, we will neglect such correlations with the contact reservoirs, which are also extremely tricky to tackle.

Truncating the hierarchy at the level of two excitations (details in Appendix B) and taking the unilateral Fourier transform ($\int_0^\infty dt e^{i\omega t}$) we obtain:

$$\begin{aligned} S_{\mathbf{q}}(t=0) &= n_{a,\mathbf{q}} = i(\omega - \omega_c(\mathbf{q}) + i\Gamma_S(\mathbf{q})) \tilde{S}_{\mathbf{q}}(\omega) + 2i\chi^*(\mathbf{q}) \tilde{Z}_{\mathbf{q}}(\omega) \\ Z_{\mathbf{q}}(t=0) &= \sum_{\mathbf{k}} Y(\mathbf{q}, \mathbf{k}) = i(\omega - \omega_{12} + i\Gamma_Z(\mathbf{q})) \tilde{Z}_{\mathbf{q}}(\omega) + i\chi(\mathbf{q}) \tilde{S}_{\mathbf{q}}(\omega) D. \end{aligned} \quad (15)$$

where $S_{\mathbf{q}}(t) = \langle a_{\mathbf{q}}^\dagger(0) a_{\mathbf{q}}(t) \rangle$, $Z_{\mathbf{q}}(t) = \sum_{\mathbf{k}} \langle a_{\mathbf{q}}^\dagger(0) c_{1,\sigma,\mathbf{k}}^\dagger c_{2,\sigma,\mathbf{k}+\mathbf{q}} \rangle$ and D represents half the difference between the total number of electrons in the fundamental subband and the number in the second one, namely:

$$D = \sum_{\mathbf{k}} D_{\mathbf{k}} = \sum_{\mathbf{k}} n_{1,\mathbf{k}} - n_{2,\mathbf{k}}. \quad (16)$$

Note that the total density of electrons is $2 \sum_{\mathbf{k}} n_{1,\mathbf{k}} + n_{2,\mathbf{k}}$, where the 2 factor accounts for the two-fold spin degeneracy of the electron states in the conduction subbands. Γ_S and Γ_Z are phenomenological damping rates for $S_{\mathbf{q}}$ and $Z_{\mathbf{q}}$ respectively. The analytical solutions are

$$\tilde{S}_{\mathbf{q}}(\omega) = \frac{in_{a,\mathbf{q}} \left(\gamma \left(\frac{\omega_c(\mathbf{q}) - \omega_{12}}{\Gamma_Y} + i \right) - (\omega - \omega_{12} + i\Gamma_Z) \right)}{(\omega - \omega_{12} + i\Gamma_Z)(\omega - \omega_c(\mathbf{q}) + i\Gamma_S) - 2\chi(\mathbf{q})^2 D}, \quad (17)$$

$$\tilde{Z}_{\mathbf{q}}(\omega) = - \frac{\chi(\mathbf{q}) S_{\mathbf{q}}(\omega) D + i \frac{\gamma n_{a,\mathbf{q}}}{2\chi(\mathbf{q})} \left(\frac{\omega_c(\mathbf{q}) - \omega_{12}}{\Gamma_Y} - i \right)}{\omega - \omega_{12} + i\Gamma_Z}.$$

The electroluminescence spectrum is simply

$$\mathcal{L}_{\mathbf{q}}(\omega) \propto \Re \tilde{S}_{\mathbf{q}}(\omega). \quad (18)$$

From the analytical result for $\tilde{S}_{\mathbf{q}}(\omega)$, we see immediately that emission spectrum is resonant at the two polariton frequencies $\omega_{\pm}(\mathbf{q})$ satisfying the equation

$$(\omega - \omega_{12} + i\Gamma_Z)(\omega - \omega_c(\mathbf{q}) + i\Gamma_S) - 2\chi(\mathbf{q})^2 D = 0. \quad (19)$$

The quantity $\Omega_R = \chi(\mathbf{q})\sqrt{2D}$ is just the vacuum Rabi frequency of the present system. At resonance (i.e.,

$\omega_c(\mathbf{q}) = \omega_{12}$), the necessary condition for the appearance of a strong coupling polaritonic splitting is $D > D_0 = \frac{(\Gamma_S - \Gamma_Z)^2}{8\chi(\mathbf{q})^2}$, meaning that the total density of electrons in the fundamental subband must be larger enough than the total density in the second. For a vacuum Rabi frequency much larger than Γ_Z and Γ_S , the minimum polariton splitting is given by twice the vacuum Rabi frequency.

Note that here the electroluminescence spectral shape does not depend explicitly on the spectral properties of the injector and extractor reservoirs. The spectrum in

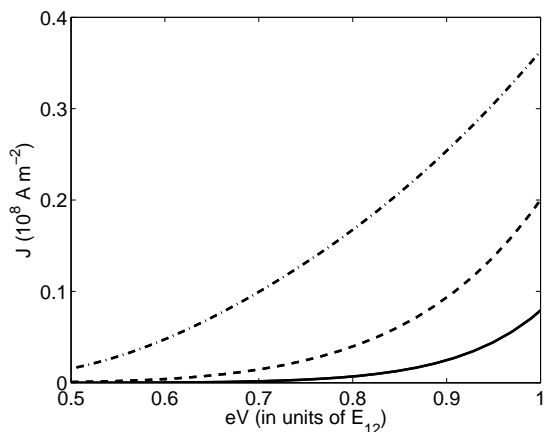


FIG. 3: Current density versus applied voltage for different values of the intersubband transition energy: $E_{12} = 50\text{meV}$, (dashed-dotted line), 100 meV (dashed line) and 150meV (solid line). Other parameters can be found in the text.

Eq. (17) has the same shape as the absorption (in presence of the same carrier densities). The dependence on the transport is only implicit, being given by the steady-state carrier and photon populations. In contrast, in the exact solution of the the simplified model of Ref. 6, it is shown that the electroluminescence spectra is the absorption spectrum times the spectral distribution of excitations in the electronic reservoir, which then acts as an electronic filter[13]. A fermionic approach based on an exact diagonalization method [14] indeed shows that the spectral properties of the electronic contact modifies significantly the spectral shape of the electroluminescence in the case of narrow band injectors. Hence, the spectrum predicted by Eq. (17) is valid only for broad band injectors. This is not really surprising because, in order to calculate the tunneling rates, we have considered bare electronic states in the quantum well and have only considered incoherent population injection and extraction processes.

V. NUMERICAL APPLICATION

Here, we apply our theory using realistic parameters for a microcavity-embedded quantum cascade electroluminescent source. In order to simplify the algebra, we have systematically neglected the photon wavevector whenever added to an electronic wavevector. Given the huge difference in the typical wavevectors of photons and electrons, this simplification is safe. Applying this approximation, we can obtain a closed set of algebraic equation where the variables are the populations in the two subbands and in the cavity photonic branch, as shown in Appendix B. This system has been solved numerically using a standard Newton method. We achieve numerical convergence in a relatively fast computation time

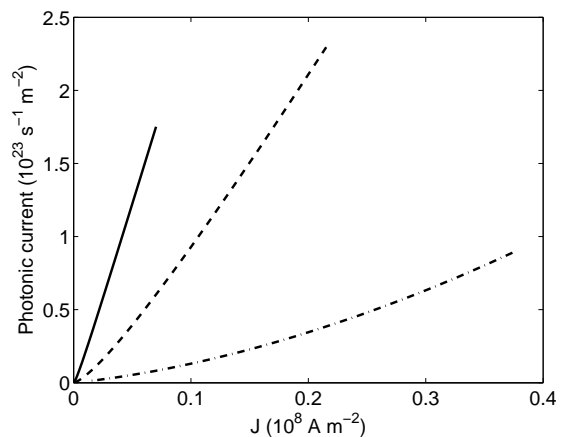


FIG. 4: Photonic current density versus electronic current for different values of the intersubband transition energy: $E_{12} = 50\text{meV}$, (dashed-dotted line), 100meV (dashed line) and 150meV (solid line). Same parameters and range of applied voltages as in Fig. 3.

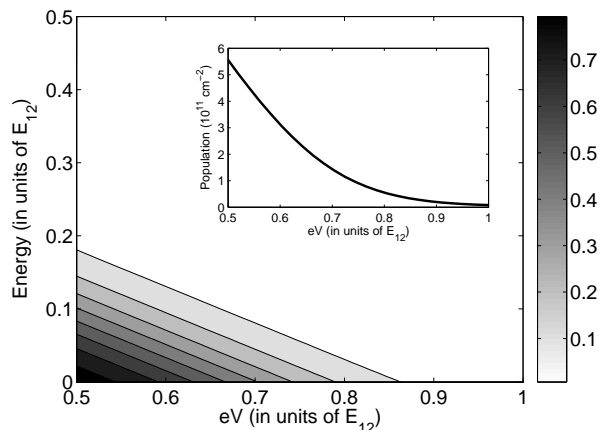


FIG. 5: Electron occupation number in the fundamental conduction subband as a function of kinetic energy and applied voltage. Inset: the integrated density of electrons in the fundamental subband versus voltage. $E_{12} = 150\text{meV}$ and other parameters as in Fig. 3. For $eV = E_{12}$, the density of electrons in the first subband is $8.3 \times 10^9\text{cm}^{-2}$.

except in the limit of vanishing bias, when the injector and extractor are strongly 'misaligned' with the two subbands. Physically in this case the steady-state situation is reached in times very long compared to the dynamics of the quantum well system, the photon population is extremely small and correspondingly the numerical method fails to converge. Anyway this is not a real limitation, because we are interested in the behavior of the system in presence of a finite voltage bias, producing a significant current flow and photonic output.

In Figs. 1 and 2, we show a sketch of the energy profile of the injector and extractor with respect to the quantum

well subbands respectively without and with an applied bias. Specifically, in the numerical calculations we have used the following electronic out-tunneling rates:

$$\Gamma_{\text{left},j,\mathbf{k}}^{\text{out}} = \frac{\Gamma e^{-\frac{(E_{0,\text{left}} - qV/2)^2}{2\sigma^2}}}{1 + e^{\beta(-\hbar\omega_{j,\mathbf{k}} + \mu_{\text{left}} - qV/2)}}, \quad (20)$$

$$\Gamma_{\text{right},j,\mathbf{k}}^{\text{out}} = \frac{\Gamma e^{-\frac{(E_{0,\text{right}} + qV/2)^2}{2\sigma^2}}}{1 + e^{\beta(-\hbar\omega_{j,\mathbf{k}} + \mu_{\text{right}} + qV/2)}},$$

where $\sigma = 0.1E_{12}$, $1/\Gamma = 0.4\text{ps}$, $E_{0,\text{left}}$ and $E_{0,\text{right}}$ are the energy offsets of the left and right minibands. The in-tunneling rates are determined by applying the relation in Eq. (10). In all the simulations, we have taken $E_{0,\text{left}} = E_{0,\text{right}} = 0.5\hbar\omega_{12}$ and $\mu_{\text{left}} = \mu_{\text{right}} = \frac{1}{3}\hbar\omega_{12}$.

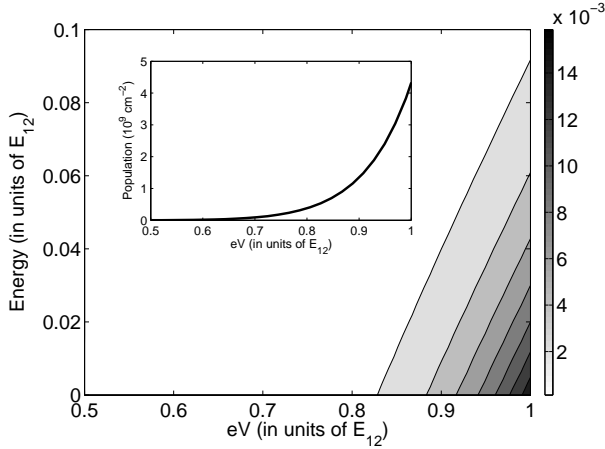


FIG. 6: Same as in Fig. 5, but for the second subband. Inset: the integrated density of electrons in the second subband versus voltage. For $eV = E_{12}$, the density of electrons in the second subband is $4.3 \times 10^9 \text{cm}^{-2}$.

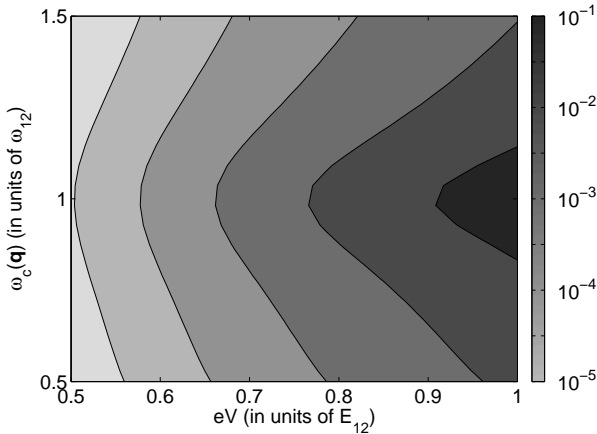


FIG. 7: Contour plot of the photon occupation (log scale) versus the applied voltage and the energy of the bare cavity photon mode.

Note that these are just phenomenological injection rates. For the amplitude Γ , we have considered values which are consistent with what realistically obtainable in semiconductor intersubband devices. Importantly, in real structures Γ can be considerably quantum engineered by changing the barrier thickness and/or the miniband structure of the injection superlattices. This is why we have not considered a very specific injector configuration and taken the simplified expression in Eq. (20) with realistic parameters.

When a voltage bias is applied, the two reservoirs are shifted symmetrically, as shown in Fig.2. In all the simulations, except when otherwise stated we used the realistic damping parameters $\Gamma_X = \Gamma_Y = \Gamma_S = \Gamma_Z = 0.1\omega_{12}$, $\gamma = 0.05\omega_{12}$, while the temperature is $T = 77\text{K}$. In the simulations we have also considered $\tau_{\mathbf{k}}$ to be independent from \mathbf{k} and such that $\frac{1}{\tau} = 0.005\omega_{12}$, except when otherwise stated. Note that here we have considered only an active quantum well. For quantum cascade structures with several active quantum wells repeated in a periodic way, the dynamics is similar and the present treatment can be generalized without major difficulties. In the simulations, the intersubband transition energy $E_{12} = \hbar\omega_{12}$ is, except where otherwise stated, equal to 150meV and the coupling constant $\chi(\mathbf{q})$ is such that the vacuum Rabi frequency is $0.1\omega_{12}$ for an electron density of $5 \times 10^{11} \text{cm}^{-2}$ (all in the fundamental subband). When E_{12} is changed, the coupling constant is adjusted in order to keep the ratio between the vacuum Rabi frequency and transition frequency constant. The effective mass m^* has been taken to be one tenth of the bare electronic mass. In the numerical calculations, the cavity spacer dielectric constant is $\epsilon_r = 10$. For each simulation, the resonance in-plane wavevector q_{res} , given by the condition $\omega_c(q_{\text{res}}) = \omega_{12}$, corresponds to an internal cavity photon propagation angle θ_{res} equal to 70 degrees, where $\tan \theta_{\text{res}} = q_{\text{res}}/q_z$.

In Fig. 3, we show the current density versus applied voltage (between the injector and extractor) for different values of E_{12} . The current-voltage profile is characteristic of an unipolar quantum cascade light emitting diode. The current grows superlinearly in the voltage region where the injector Fermi level approaches the second subband. The current is bigger for smaller E_{12} because, keeping the injection rate Γ constant (but all the internal rates of the system proportional to E_{12}), the injection and extraction processes become the dominant processes. Note that an increase of the nonradiative relaxation rate $1/\tau$ produces a nearly proportional increase of the electronic current (not shown). The rates of emitted photons per unit area (integrated all over the in-plane wavevectors) are shown in Fig. 4 as a function of the flowing current, showing an approximately linear behavior.

Fig. 5 and 6 show contour plots of the electron occupation numbers of the first and second subband respectively as a function of the applied voltage and of the kinetic energy. The insets in Fig. 5 and 6 show respectively the integrated density of electrons in the first and sec-

ond subband. It is apparent that with increasing voltage the population in the first subband decreases, while the population in the second subband increases.

When the injector Fermi level becomes aligned with the second subband, as expected, the carrier occupation numbers in the two subbands are considerably out of equilibrium. The decrease of the first subband carrier occupation numbers is beneficial for the radiative efficiency of the spontaneous emission, because the influence of Pauli blocking is reduced. Moreover, in the considered conditions, the density of electrons in the first subband is still considerably larger than in the second subband, thus producing a large vacuum Rabi coupling and efficient emission rate.

Fig. 7 contains a contour plot of the cavity photon occupation number versus the bare photon energy, showing that the maximum of emission is obtained when the bare photon energy is resonant with the intersubband transition, as expected and as observed experimentally [13, 18]. With the considered parameters, the density of electrons in the first subband is high enough to be in the strong coupling regime, as depicted in Fig. 8, where the anticrossing of two polariton branches is clearly present. The minimum polariton splitting, given by the expression $2\chi(q)\sqrt{2D}$ is reported in Fig. 9 as a function of the applied bias. With increasing voltage, the population difference $D = \sum_{\mathbf{k}} D_{\mathbf{k}} = \sum_{\mathbf{k}} n_{1,\mathbf{k}} - n_{2,\mathbf{k}}$ diminishes. This results in a decrease of the vacuum Rabi frequency and consequently of the polariton splitting. This high-excitation feature has been already observed in experiments [13, 18] and can not be described within a bosonic approach [6], which can be applied only to the low excitation density case [20].

It is interesting to analyze the quantum efficiency η , defined as the ratio between the photonic emission rate and the electronic current, namely

$$\eta = \frac{2\gamma \sum_{\mathbf{q}} n_{a,\mathbf{q}}}{\sum_{\mathbf{k}} \Gamma_{1,\mathbf{k}}^{\text{out}} n_{1,\mathbf{k}} - \Gamma_{1,\mathbf{k}}^{\text{in}} (1 - n_{1,\mathbf{k}})}. \quad (21)$$

In Fig. 10, we plot the quantum efficiency η at $eV = E_{12}$ versus the vacuum Rabi frequency Ω_R at the same voltage (log-log scale). In the simulations, the vacuum Rabi frequency has been varied by changing the coupling constant $\chi(\mathbf{q})$. In a realistic quantum engineered device, $\chi(\mathbf{q})$ can be tailored in different ways. For example, by growing the active quantum wells in a spatial region where the cavity mode field is very small, it is possible to quench dramatically the value of $\chi(\mathbf{q})$. Moreover, by using different shape of quantum wells, it is also possible to tailor the transition dipole d_{12} . Fig. 10 shows that in the weak coupling regime (small values of Ω_R) the efficiency grows like Ω_R^2 . In the strong coupling regime, the efficiency becomes impressive and then tends to saturate. It is apparent that the radiative efficiency smoothly increases passing from the weak to the strong coupling regime. This crossover occurs because the radiative efficiency depends on the spectrally integrated emission and

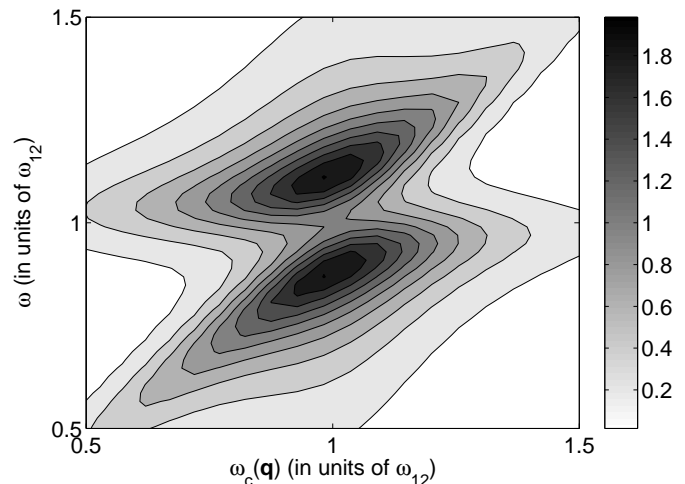


FIG. 8: Contour plot of the electroluminescence (arb. units) as a function of the bare cavity photon energy $\omega_c(q)$ and of the emission frequency ω for an applied voltage $eV = 0.5E_{12}$. The anticrossing of the two intersubband polariton branches is apparent in electroluminescence spectra.

it is therefore insensitive to the sudden appearance of the polariton doublet in the strong coupling emission spectra.

This results are in qualitative agreement with the analytical solutions of the simplified model in Ref. 6, where only the bright intersubband states are considered and where the electronic reservoir is modeled with a bath of harmonic oscillators. As shown in Fig. 11, the nonradiative population relaxation rate $1/\tau$ has the most significant effect. In the considered regime of parameters, the efficiency is proportional to τ .

It is interesting to compare our results for this microcavity system with the standard free space case. In the free-space case, the photon current, obtained by applying the Fermi golden rule, is given by the formula $P = \frac{2d_{12}^2\omega_{12}^3\sqrt{\epsilon_r}}{3\pi c^3\hbar\epsilon_0} \sum_{\mathbf{k}} n_{2,\mathbf{k}}(1 - n_{1,\mathbf{k}})$. As it is well known, the free-space radiative efficiency dramatically decreases with the intersubband emission wavelength due to the $\omega_{12}^3 d_{12}^2$ dependence of the spontaneous emission rate ($d_{12}^2 \propto 1/\omega_{12}$, so the spontaneous emission rate scales effectively as ω_{12}^2). In the mid-infrared, by using the same parameters, for a transition of 150 meV, the quantum efficiency is of the order of $10^{-4} - 10^{-5}$. Hence, it is clear from our results that a strong coupling light-emitting diode based on a planar microcavity system can provide a dramatic enhancement with respect to the free space case (even three orders of magnitude for the larger vacuum Rabi frequency case).

VI. CONCLUSIONS AND PERSPECTIVES

In conclusion, we have presented a quantum theoretical study of the quantum well intersubband electrolumi-

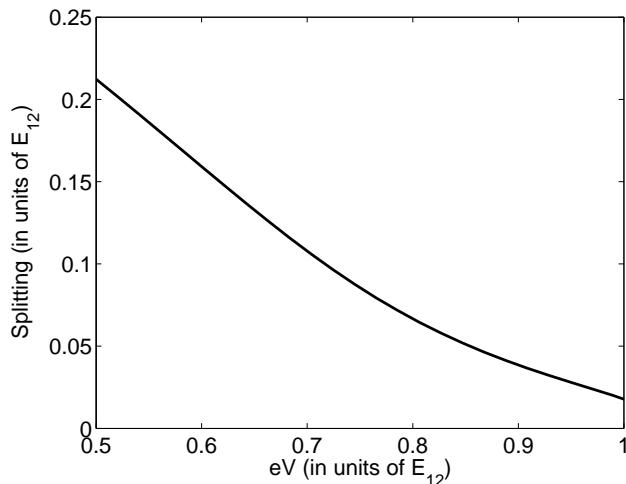


FIG. 9: Minimum polariton splitting as a function of the applied voltage. $E_{12} = 150\text{meV}$ and other parameters can be found in the text.

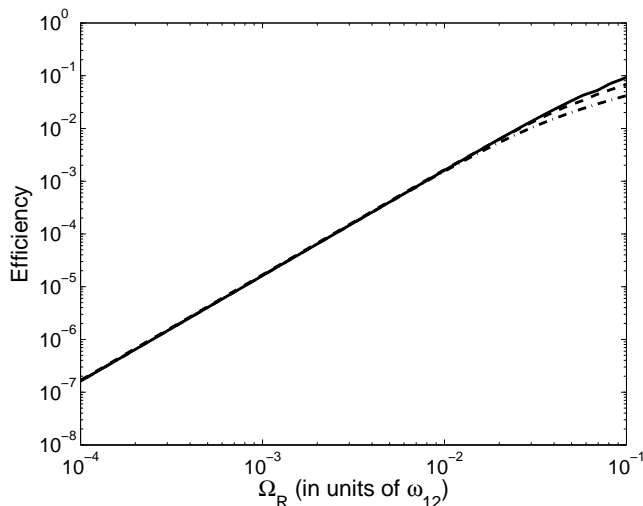


FIG. 10: Quantum efficiency versus the corresponding vacuum Rabi frequency at the voltage $eV = E_{12}$. The three lines are obtained with different values of the coherence damping coefficients: $\Gamma_X = \Gamma_Y = 0.1\omega_{12}$ (solid line), $0.05\omega_{12}$ (dashed line) and $0.025\omega_{12}$ (dashed-dotted line). $E_{12} = 150\text{meV}$.

nescence from a semiconductor microcavity in the incoherent transport regime, i.e. when the coupling to the electronic contacts concerns only the electron populations. The problem has been tackled starting from the fermionic electron Hamiltonian for the two-subbands and by using a cluster factorization method to truncate the infinite hierarchy of dynamical equations for the relevant expectation values of operator products. At the present level of approximation, we have been able to describe the incoherent electron transport through the dynamics

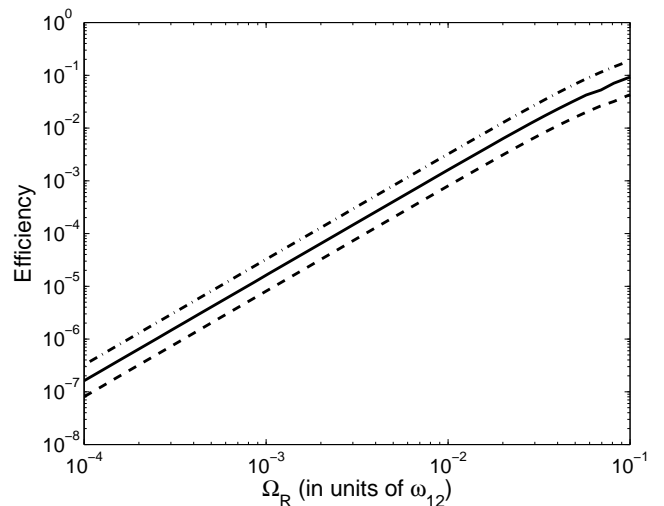


FIG. 11: Quantum efficiency versus the corresponding vacuum Rabi frequency at the voltage $eV = E_{12}$. The three lines are obtained with different values of the non-radiative relaxation rate: $\frac{1}{\tau} = 0.01\omega_{12}$ (dashed line), $0.005\omega_{12}$ (solid line) and $0.0025\omega_{12}$ (dashed-dotted line). $E_{12} = 150\text{meV}$.

of the electronic subband populations and the electroluminescence through the dynamics of the cavity photon population, which is coupled to the correlations between the electromagnetic field and the intersubband polarization. We have discussed the limits of applicability of the present approach, which neglects the impact of the vacuum Rabi coupling on the quantum well carrier spectral function and any correlation between the quantum well and the contact reservoirs. The analogies and differences with the exact predictions of the simplified model in Ref. 6 have been critically and extensively discussed. We have shown the appearance of cavity polariton resonances in the emission spectra, when a large density of electrons occupies the fundamental subband. We have described how the vacuum Rabi splitting decreases with increasing voltage and described the photonic output in the different transport conditions. Our results show that even in presence of non-radiative relaxation and Pauli blocking, the quantum efficiency of the microcavity intersubband electroluminescence can be considerably enhanced by increasing the vacuum Rabi frequency. A more refined treatment[14] based on a fermionic exact diagonalization method shows that under certain conditions the strong vacuum Rabi coupling regime affect considerably not only the dynamics of the intersubband polarization (hence the absorption spectrum), but also the quantum well electron spectral properties and consequently the tunneling transport using narrow-band injectors. As future perspective, this could be exploited to further improve the quantum efficiency of microcavity intersubband emitters and for the eventual realization of intersubband polariton lasers.

Acknowledgments

We are pleased to thank I. Carusotto, R. Colombelli, L. Sapienza, C. Sirtori, A. Vasanelli for discussions.

APPENDIX A: FACTORIZATIONS

As stated in the main body of the paper we used a cluster expansion and truncation scheme to obtain a closed set of equations. Here we briefly review the principles of this method following [15, 16, 17] and apply it to the actual case.

If we consider each bosonic operator or each pair of fermionic operators as an excitation operator and we write the expectation value of an N excitation operator as $\langle N \rangle$, then the Heisenberg equation of motion takes the form:

$$i \frac{\partial}{\partial t} \langle N \rangle = T[\langle N \rangle] + V[\langle N + 1 \rangle]$$

where the N -excitation expectation value is coupled to higher order quantities via the functional V . An N -excitation truncation scheme is obtained if we factorize all the expectation values of more than N excitation in all the possible ways and considering the sign exchange for the fermionic operators in order to obtain a factorized quantity that respects the commutation and anticommutation properties of the original quantity.

We are interested in incoherent emission only, so the only nonzero one excitation operators we consider are $\langle c_{1,\sigma,\mathbf{k}}^\dagger c_{1,\sigma,\mathbf{k}} \rangle$ and $\langle c_{2,\sigma,\mathbf{k}}^\dagger c_{2,\sigma,\mathbf{k}} \rangle$. We factorized the 3 excitations operators in the following way:

$$\begin{aligned} \langle a_{\mathbf{q}} c_{1,\sigma,\mathbf{k}} c_{2,\sigma,\mathbf{k}'}^\dagger c_{2,\sigma',\mathbf{k}''}^\dagger c_{2,\sigma',\mathbf{k}'''} \rangle &= - \langle a_{\mathbf{q}} c_{2,\sigma,\mathbf{k}'}^\dagger c_{1,\sigma,\mathbf{k}} \rangle \langle c_{2,\sigma',\mathbf{k}''}^\dagger c_{2,\sigma',\mathbf{k}'''} \rangle + \langle a_{\mathbf{q}} c_{2,\sigma',\mathbf{k}''}^\dagger c_{1,\sigma,\mathbf{k}} \rangle \langle c_{2,\sigma,\mathbf{k}'}^\dagger c_{2,\sigma',\mathbf{k}'''} \rangle \\ &= - \langle a_{\mathbf{q}} c_{2,\sigma,\mathbf{k}'}^\dagger c_{1,\sigma,\mathbf{k}} \rangle \delta_{\mathbf{k}'',\mathbf{k}'''} n_{2,\mathbf{k}''} + \langle a_{\mathbf{q}} c_{2,\sigma,\mathbf{k}''}^\dagger c_{1,\sigma,\mathbf{k}} \rangle \delta_{\mathbf{k}',\mathbf{k}'''} \delta_{\sigma,\sigma'} n_{2,\mathbf{k}'} \\ \langle a_{\mathbf{q}} c_{2,\sigma,\mathbf{k}}^\dagger c_{1,\sigma,\mathbf{k}'} c_{1,\sigma',\mathbf{k}''}^\dagger c_{1,\sigma',\mathbf{k}'''} \rangle &= - \langle a_{\mathbf{q}} c_{2,\sigma,\mathbf{k}}^\dagger c_{1,\sigma',\mathbf{k}''} \rangle \langle c_{1,\sigma,\mathbf{k}'}^\dagger c_{1,\sigma',\mathbf{k}'''} \rangle + \langle a_{\mathbf{q}} c_{2,\sigma,\mathbf{k}}^\dagger c_{1,\sigma,\mathbf{k}'} \rangle \langle c_{1,\sigma',\mathbf{k}''}^\dagger c_{1,\sigma',\mathbf{k}'''} \rangle \\ &= - \langle a_{\mathbf{q}} c_{2,\sigma,\mathbf{k}}^\dagger c_{1,\sigma,\mathbf{k}''} \rangle \delta_{\mathbf{k}',\mathbf{k}'''} \delta_{\sigma,\sigma'} (1 - n_{1,\mathbf{k}'}) + \langle a_{\mathbf{q}} c_{2,\sigma,\mathbf{k}}^\dagger c_{1,\sigma,\mathbf{k}'} \rangle \delta_{\mathbf{k}'',\mathbf{k}'''} (1 - n_{1,\mathbf{k}''}) \end{aligned}$$

For the two-time quantities in the calculation of luminescence spectrum, we proceed analogously and obtain:

$$\begin{aligned} \langle a_{\mathbf{q}}^\dagger(0) a_{\mathbf{q}'} c_{2,\sigma,\mathbf{k}+\mathbf{q}}^\dagger c_{2,\sigma,\mathbf{k}+\mathbf{q}'} \rangle &= \langle a_{\mathbf{q}}^\dagger(0) a_{\mathbf{q}'} \rangle \langle c_{2,\sigma,\mathbf{k}+\mathbf{q}}^\dagger c_{2,\sigma,\mathbf{k}+\mathbf{q}'} \rangle \delta_{\mathbf{q},\mathbf{q}'}, \\ \langle a_{\mathbf{q}}^\dagger(0) a_{\mathbf{q}'} c_{1,\sigma,\mathbf{k}}^\dagger c_{1,\sigma,\mathbf{k}+\mathbf{q}-\mathbf{q}'} \rangle &= \langle a_{\mathbf{q}}^\dagger(0) a_{\mathbf{q}'} \rangle \langle c_{1,\sigma,\mathbf{k}}^\dagger c_{1,\sigma,\mathbf{k}+\mathbf{q}-\mathbf{q}'} \rangle \delta_{\mathbf{q},\mathbf{q}'}. \end{aligned}$$

APPENDIX B: ALGEBRAIC EQUATIONS FOR THE STEADY-STATE REGIME

In the steady-state regime, neglecting the photonic wavevector into sums over electronic wavevectors, the system of equations (7) reduces to the following system of algebraic equations.

$$\begin{aligned} 0 &= \left(B_{\mathbf{q}}(\gamma + \Gamma_X) + \left(\frac{\delta_{\mathbf{q}}^2}{\Gamma_Y} + \frac{G_{\mathbf{q}} \Gamma_X}{2D\chi(\mathbf{q})^2} \right) \gamma \right) n_{a,\mathbf{q}} + \frac{B_{\mathbf{q}}}{D} \sum_{\mathbf{k}} (1 - D_{\mathbf{k}}) \left(\frac{n_{1,\mathbf{k}} - n_{1,\mathbf{k}}^0}{\tau_{\mathbf{k}}} + \Gamma_{1,\mathbf{k}}^{out} n_{1,\mathbf{k}} - \Gamma_{1,\mathbf{k}}^{in} (1 - n_{1,\mathbf{k}}) \right) - \frac{2B_{\mathbf{q}} F \Gamma_X}{D}, \\ 0 &= \left(\sum_{\mathbf{q}} \frac{B_{\mathbf{q}} \chi(\mathbf{q})^2}{G_{\mathbf{q}} \Gamma_X} (1 - D_{\mathbf{k}}) + \frac{1}{2} \right) \left(\frac{n_{1,\mathbf{k}} - n_{1,\mathbf{k}}^0}{\tau_{\mathbf{k}}} + \Gamma_{1,\mathbf{k}}^{out} n_{1,\mathbf{k}} - \Gamma_{1,\mathbf{k}}^{in} (1 - n_{1,\mathbf{k}}) \right) \\ &\quad + \frac{D_{\mathbf{k}}}{\Gamma_X \Gamma_Y} \sum_{\mathbf{q}} \frac{\chi(\mathbf{q})^2 n_{a,\mathbf{q}}}{G_{\mathbf{q}}} (\Gamma_Y B_{\mathbf{q}}(\gamma + \Gamma_X) + \delta_{\mathbf{q}}^2 \gamma) - 2F_{\mathbf{k}} \sum_{\mathbf{q}} \frac{B_{\mathbf{q}} \chi(\mathbf{q})^2}{G_{\mathbf{q}}}, \\ 0 &= - \frac{n_{2,\mathbf{k}} - n_{2,\mathbf{k}}^0}{\tau_{\mathbf{k}}} - \Gamma_{2,\mathbf{k}}^{out} n_{2,\mathbf{k}} + \Gamma_{2,\mathbf{k}}^{in} (1 - n_{2,\mathbf{k}}) - \frac{n_{1,\mathbf{k}} - n_{1,\mathbf{k}}^0}{\tau_{\mathbf{k}}} - \Gamma_{1,\mathbf{k}}^{out} n_{1,\mathbf{k}} + \Gamma_{1,\mathbf{k}}^{in} (1 - n_{1,\mathbf{k}}), \end{aligned}$$

where

$$\begin{aligned}
D_{\mathbf{k}} &= n_{1,\mathbf{k}} - n_{2,\mathbf{k}} \\
F_{\mathbf{k}} &= n_{2,\mathbf{k}}(1 - n_{1,\mathbf{k}}) \\
D &= \sum_{\mathbf{k}} D_{\mathbf{k}} \\
F &= \sum_{\mathbf{k}} F_{\mathbf{k}} \\
n_{1,\mathbf{k}}^0 &= \frac{1}{\exp \beta(\omega_1(\mathbf{k}) - \epsilon_F) + 1} \\
n_{2,\mathbf{k}}^0 &= \frac{1}{\exp \beta(\omega_2(\mathbf{k}) - \epsilon_F) + 1} \\
B_{\mathbf{q}} &= \Gamma_Y + \frac{2\chi(\mathbf{q})^2}{\Gamma_X} D \\
\delta_{\mathbf{q}} &= \omega_c(\mathbf{q}) - \omega_{12} \\
G_{\mathbf{q}} &= (\omega_c(\mathbf{q}) - \omega_{12})^2 + (\Gamma_Y + \frac{2\chi(\mathbf{q})^2 D}{\Gamma_X})^2.
\end{aligned}$$

ϵ_F is calculated by inverting the relation

$$\sum_{\mathbf{k}} n_{1,\mathbf{k}} + n_{2,\mathbf{k}} = \frac{m^*}{2\pi\hbar^2} \int_0^\infty d\epsilon \frac{1}{\exp \beta(\epsilon - \epsilon_F) + 1} + \frac{1}{\exp \beta(\epsilon + E_{12} - \epsilon_F) + 1}.$$

Discretizing the electronic and photonic wavevectors on a grid of respectively $N_{\mathbf{k}}$ and $N_{\mathbf{q}}$ points, we have a system of $2N_{\mathbf{k}} + N_{\mathbf{q}}$ equations that can be numerically solved, e.g., with a Newton algorithm.

-
- [1] *Intersubband Transitions in Quantum Wells: Physics and Device Applications I*, edited by H. C. Liu and F. Capasso, Semiconductors and Semimetals Vol. 62 (Academic Press, San Diego, 2000).
 - [2] D. Dini, R. Kohler, A. Tredicucci, G. Biasiol, and L. Sorba, Phys. Rev. Lett. **90**, 116401 (2003).
 - [3] A. A. Anappara, A. Tredicucci, G. Biasiol, L. Sorba, Appl. Phys. Lett. **87**, 051105 (2005).
 - [4] A. A. Anappara, A. Tredicucci, F. Beltram, G. Biasiol, L. Sorba, Appl. Phys. Lett. **89**, 171109 (2006).
 - [5] C. Ciuti, G. Bastard, I. Carusotto, Phys. Rev. B **72**, 115303 (2005).
 - [6] C. Ciuti, I. Carusotto, Phys. Rev. A **74**, 033811 (2006).
 - [7] S. De Liberato, C. Ciuti, I. Carusotto, Phys. Rev. Lett. **98**, 103602 (2007).
 - [8] J. Faist, F. Capasso, D.L. Sivco, C. Sirtori, A. L. Hutchinson, A.Y. Cho, Science **264**, 5553 (1994).
 - [9] R. Köhler, A. Tredicucci, F. Beltram, H.E. Beere, E.H. Linfield, A.G. Davies, D.A. Ritchie, R.C. Iotti, F. Rossi, Nature **417**, 156 (2002).
 - [10] R. Colombelli, K. Srinivasan, M. Troccoli, O. Painter, C. F. Gmachl, D. M. Tennant, A. M. Sergent, D. L. Sivco, A. Y. Cho, F. Capasso, Science **302**, 1374 (2003).
 - [11] R. Colombelli, C. Ciuti, Y. Chassagneux, C. Sirtori, Semicond. Sci. Technol. **20**, 985 (2005).
 - [12] L. Sapienza, A. Vasanelli, C. Ciuti, C. Manquest, C. Sirtori, R. Colombelli, and U. Gennser, Appl. Phys. Lett. **90**, 201101 (2007).
 - [13] L. Sapienza, A. Vasanelli, R. Colombelli, C. Ciuti, Y. Chassagneux, C. Manquest, U. Gennser, C. Sirtori, Phys. Rev. Lett. **100**, 136806 (2008).
 - [14] S. De Liberato and C. Ciuti, arxiv:0802.4091.
 - [15] J. Fricke, Ann. Phys. **252**, 479 (1996).
 - [16] J. Fricke, V. Meden, C. Wohler, K. Schonhammer, Ann. Phys. **253**, 177 (1997).
 - [17] M. Kira, W. Hoyer, T. Stroucken, S. W. Koch, Phys. Rev. Lett. **87**, 176401 (2001).
 - [18] L. Sapienza, (Ph. D. thesis, University of Paris 7, 2007).
 - [19] D. E. Nikonov, A. Imamoglu, L. V. Butov, and H. Schmidt, Phys. Rev. Lett. **79**, 4633 (1997).
 - [20] M. F. Pereira, Jr., Phys. Rev. B **75**, 195301, (2007).